JCTC Journal of Chemical Theory and Computation

Theoretical Conformational Analysis for Neurotransmitters in the Gas Phase and in Aqueous Solution. Serotonin

Giuliano Alagona,*,† Caterina Ghio,† and Peter I. Nagy*,‡

Molecular Modeling Lab, CNR-IPCF, Institute for Physical Chemistry Processes, Via Moruzzi 1, I-56124 Pisa, Italy, and Department of Medicinal and Biological Chemistry and Center for Drug Design and Development, The University of Toledo, Toledo, Ohio 43606-3390

Received April 5, 2005

Abstract: Conformational analyses have been performed for protonated serotonin in the gas phase, aqueous solution, and in the binding cavity of a 5-HT2A receptor model. DFT geometry optimizations have been performed in the gas phase at the B3LYP/6-31G* levels. Optimized calculations up to the B3LYP/6-311++G** level find two low-energy gauche conformations separated by 8−10 kcal/mol barriers from a trans conformation with relative energy of about 6 kcal/mol. In aqueous solution as concluded from IEF-PCM/B3LYP/6-31G* and IEF-PCM/MP2/6-31G*//IEF-PCM/B3LYP/6-31G* continuum solvent calculations as well as Monte Carlo free energy perturbation simulations with explicit solvent molecules, those barriers decrease to 2−7 kcal/mol, while the two gauche and one trans conformers are within a 3 kcal/mol relative free energy range. The solute is strongly hydrated by about three water molecules around the $-NH_3^+$ group and by one water molecule for each of the pyrrole and phenolic hydrogen atoms. Docking studies of the protonated ligand predicted both gauche and trans ligand conformers to favorably interact with the 5-HT2A receptor in its hypothesized binding cavity. The theoretical studies confirm the experimental results regarding strong interactions with the Asp155 and Ser159 residues (TM helix III) and the interactions of the indole ring with Phe, Trp, and Tyr side chains in TM V, VI, and VII helices within a 24 kcal/mol range for the relative interaction energies.

I. Introduction

The present study is a continuation of our interest toward the in-solution structure of biogen amine neurotransmitters. After former studies for histamine,[1] dopamine,[2] and norepinephrine[3] by us and others, the present target of our investigation is serotonin (5-hydroxytryptamine, 5-HT). In CNS, serotonin has a neurotransmitter function on different 5-HT receptor subtypes, influencing numerous physiological processes such as sleep, cognition, motor activity, temperature regulation, nociception, appetite, sexual behavior, etc. In periphery, serotonin plays role as a regulator of smooth muscle function in the cardiovascular and gastrointestinal systems and also in platelet aggregation.

The neutral, gas-phase serotonin has been theoretically studied recently by Van Mourik and Emson.[4] The biogen amine neurotransmitters above are primarily protonated, however, in aqueous solution at the physiological tissue pH = 7.4,[3a] and according to a widely accepted concept,[5] this cationic form is the acting one as an agonist for the corresponding G-protein coupled receptor (GPCR).[6] GPCRs are transmembrane receptors comprising a densely packed seven-helix system, and using the recently determined rhodopsin receptor[7] as a template for their model, the binding sites are located about 11 Å away from their extracellular surfaces, down along the main axes of the helices.

* Corresponding authors phone: +39-050-3152450; fax: +39-050-3152442; e-mail: G.Alagona@ipcf.cnr.it (G.A.) and phone: (419)530-1945; fax: (419)530-1909; e-mail: pnagy@utnet.utoledo.edu (P.I.N.).

† CNR-IPCF, Institute for Physical Chemistry Processes.

‡ The University of Toledo.

10.1021/ct050088c CCC: $30.25
Published on Web 07/20/2005

One of the most important questions is the following: how does the cationic neurotransmitter reach the binding cavity from the synaptic cleft, which may be essentially characterized as an aqueous solution. This mechanism has not been explored yet. Accordingly, we address two questions in the present study. The focus of our interest is to find the prevalent conformers of serotonin in aqueous solution mimicking the extracellular environment in the synaptic cleft. The low-energy serotonin conformers, as starting models for the bound form for the agonist of the 5-HT2A serotonin receptor, will be utilized in simple molecular mechanics docking studies. In these latter studies our goal is to explore whether the agonist has to undergo remarkable conformational changes as compared to its favored in-solution structure, to fit optimally to the amino acid side chains in the binding cavity.

For histamine, dopamine, and norepinephrine as well as for serotonin the protonation is a reversible process and depends on the chemical character of the environment. The protonated state of these molecules must be thermodynamically stable in the aqueous extracellular environment at the physiological tissue pH (see above). Considering, however, the narrow pore in the seven-helix transmembrane structure of the GPCRs, it is an essential question whether the protonated form is maintained throughout the traverse process from the receptor surface to the binding cavity at a depth of about 11 Å. Since there is no space for accommodating a large number of water molecules in the pore, it is also possible that the proton is lost throughout the traverse process and is regained in the binding cavity. In fact, our computer modeling for the complex of the norepinephrine ligand with the β-adrenergic receptor indicates that a few water molecules can be accommodated in the binding cavity even in the presence of the agonist.[3a]

Common in the binding of these neurotransmitters is that there is an ion-pair interaction with the protonated nitrogen of the agonist and the negatively charged Asp 3.32 side chain (using the Ballesteros−Weinstein numbering scheme[8] for the receptor residues) in transmembrane III. This interaction anchors the ligand, and if there are at least two water molecules in the neighborhood or the local dielectric constant is larger than nine, the environment helps maintain the ion-pair structure.[9] On this basis, a conformational study of protonated serotonin seems to be justified, and the present investigation explores the relevant part of the in-solution conformational space by utilizing continuum dielectric and Monte Carlo methods in combination with ab initio and density functional theory calculations.

II. Methods and Calculations

Atom numbering and the three main conformations, G1, G2 gauche, and T trans, for protonated serotonin are shown in Scheme 1. The minimum energy OH arrangement has been determined from the flexible scan of the $H_5O_5C_5C_6$ (φ_4) dihedral angle at the DFT level by applying the B3LYP functional[10] using the 6-31G* basis set[11] for G1, G2, and T in the gas-phase. Single point MP2 calculations[12] have been carried out for comparison. A potential energy surface (PES) was calculated changing the $C_2C_3C_\beta C_\alpha$ (φ_1) and the $C_3C_\beta C_\alpha N$ (φ_2) torsion angles in 30° increments at the same level and

Scheme 1. G1, T, and G2 Protonated Serotonin

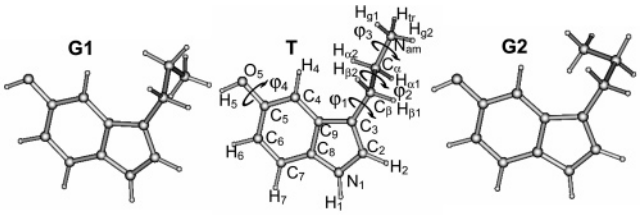

optimizing the rest of the internal coordinates. Three local minima and three transition states (TS), verified by frequency analysis, were identified on the ($0° \le \varphi_1 \le 180°$) PES. Since the rotation of the serotonin side chain is possible both clockwise and counterclockwise, there is a mirror image for each structure with equal energy. The PES reflects this character upon 360° rotation of both the φ_1 and φ_2 torsion angles and possesses C_2 symmetry, accordingly. The relative energies for the local minima and TS calculated through gas-phase optimizations at the B3LYP/6-31G* and B3LYP/6-311++G** levels have been compared. The calculations were carried out using the Gaussian 03 software[13] running in Pisa.

Using thermal corrections, the relative molar internal free energies for the selected conformers, ΔG(int), were calculated at $T = 310$ K and $p = 1$ atm, using the rigid rotator-harmonic oscillator approximation.[14] Accordingly, the molar ΔG(int) was calculated as

$$\Delta G(\text{int}) = \Delta E + \Delta G_{\text{th}}(T) = \Delta E + \Delta\text{ZPE} + \Delta(H(T) - \text{ZPE}) - T\Delta S(T) \quad (1)$$

Here ΔE and ΔG_{th}(T) are the quantum chemically calculated internal energy difference and the so-called thermal correction, respectively. Contributions to the latter, ZPE, $H(T)$, and $S(T)$, are the zero point energy, the vibrational enthalpy, and the total entropy at T (= 310 K), respectively. Since the proposed scaling factor for the B3LYP/6-31G* ΔZPE correction[15] (0.9804) is very close to 1, no scaling factor was applied.

In-solution calculations started with B3LYP/6-31G* geometry optimizations at the integral-equation-formalism (IEF)-PCM level. In the IEF-PCM framework,[16] the solvent is represented by a continuous medium characterized by its dielectric permittivity, where the solute is embedded inside a cavity of proper shape created around it. The cavity, built according to the actual geometric structure of the solute, univocally defines the closed surface that separates solute from solvent, used to formulate the basic electrostatic equations characterizing the solute−solvent (su−sv) system. Bondi radii[17] have been used throughout, except for the united atom description of the CH (R=1.9 Å) and CH_2/CH_3 (R=2.0 Å) groups, applying a 1.2 scaling factor. In addition to computational efficiency, a prominent advantage of the IEF-PCM approach with respect to standard PCM[18] is that errors, such as those linked to the partition of the continuous apparent surface charge into discrete elements and to the electronic charge escaped outside the cavity, are reduced at least by an order of magnitude, because of the use of operators related to the electric potential instead of the electric field.[19]

Starting from gas-phase optimized geometries, structures corresponding to energy minima and TSs were optimized in aqueous solution. In addition to these structures, six further structures, called midpoints henceforth, were optimized, while the $C_2C_3C_\beta C_\alpha$ and $C_3C_\beta C_\alpha N$ torsion angles were kept fixed at values taken as averages of those related to the two closest stationary points. [Only in the case of midpoint 1, because of the shape of the PES, it was necessary to optimize φ_1 at φ_2 = average of the corresponding value for G1 and TS1 structures.] Then all other internal coordinates were relaxed. Employing this strategy, a route connecting the extreme points of the in-solution PES was selected. Since we are interested in the relative free energies only for points G1, TS1, G2, TS2, T, and TS3, the calculated values are independent of the selected paths to connect the six points mentioned. The IEF-PCM relative free energies were calculated as

$$\Delta G_{tot} = \Delta E^{s}_{int} + 1/2\Delta E_{susv} + \Delta G_{drc} \quad (2)$$

The first two energy terms were obtained by the iterative solution of the Schrödinger equation for a solute immersed in a polarizable continuum dielectric.

$$E^{s}_{int} = [<\Psi_s|H^\circ|\Psi_s>] \quad (3a)$$

$$E_{susv} = [<\Psi_s|V_R^{sol}|\Psi_s>] \quad (3b)$$

H° is the solute Hamiltonian, V_R^{sol} is the solvent reaction field generated by the fully polarized solute in solution, and Ψ_s is the converged wave function of the solute. The G_{drc} term stands for the nonelectrostatic, dispersion-repulsion-cavity part of the free energy of the solute in solution. $C_3C_\beta C_\alpha N$ rotational potential curves in solution have been calculated at different levels and with different basis sets for the serotonin cation. Local energy minima and transition states in solution were verified by frequency analysis. Vibrational frequencies at the IEF-PCM/B3LYP/6-31G* level have been computed.

By utilizing the IEF-PCM/B3LYP/6-31G* optimized molecular structures, the procedure we proposed recently[20] has been followed: electrostatic potential fitted CHELPG[21] and RESP[22] charges were derived, using the IEF-PCM/B3LYP/6-31G* wave function, for the 26 atoms of the solute in 12 conformations. These atomic charges were applied in Monte Carlo (MC) simulations and in docking studies when a model receptor was considered. Relative conformational solvation free energies were obtained by using the free energy perturbation method (FEP)[23a] as implemented in Monte Carlo simulations.[23b] Calculations were carried out by the use of the BOSS 4.2 software.[24]

MC simulations[25] for the aqueous solution of a protonated neurotransmitter was described in our earlier study for norepinephrine.[3a] Therefore, only the main points and the important differences as compared to the present modeling will be described here. MC simulations for the serotonin cation were performed in NpT (isobaric−isothermal) ensembles at T = 310 K and p = 1 atm. A water box, including 485 TIP4P water molecules[26] and a single solute with or without a chloride counterion, was considered for the aqueous solution model. Solvation free energy changes were calculated for rotation about the $C_\beta-C_\alpha$ axis. Geometries of the reference structures with fixed changes of ∼30° in the reaction path torsion angle were determined from IEF-PCM/B3LYP/6-31G* calculations relaxing all other internal coordinates. The interaction energy of the solution elements was calculated using the all-atom 12-6-1 OPLS-AA pair potential.[27] Steric OPLS parameters were taken from the program library, while potential derived charges were obtained as stated above.

Three different MC simulations in which the $-NH_3^+$ group, as a unit, was rotated by 360° about the $C_\beta-C_\alpha$ axis were carried out. The CHELPG charge set was applied for the $SerH^+\cdots Cl^-$ ion pair; the RESP fitted atomic charges were used for the single-solute serotonin cation ($SerH^+$) and the $SerH^+\cdots Cl^-$ ion pair. Application of a counterion is in place because the whole system (solute and its environment) must be neutral. In physiological conditions, the liquid environment can be characterized as a saline solution of 0.15 mol/dm^3 concentration. By simply assuming that the salt is NaCl and/or KCl, the concentration corresponds approximately to 1 Cl^-:360 water molecules. Our system is slightly more dilute with 1 Cl^-:485 water molecules.

In the original ion pair approximation with the CHELPG charges, the two ions were allowed to move independently. With a freely moving chloride ion, however, increments to the free energy were calculated with such a large noise that the standard deviation was regularly close to the free energy increment value itself, even for torsion angle changes as small as 0.8° and considering 5000K and 6000K configurations in the equilibration and averaging phases, respectively. These studies, however, pointed out that MC simulations predict a largely separated cation···anion system. On this basis, the $C_3\cdots Cl$ distance was kept fixed at 12 Å, meeting the requirement that Δcoord < edge/2. Nonetheless, the serotonin cation could rotate about a random axis through atom C_3, thus the relative orientation of the ion pair was not rigid. The solute−solvent and solvent−solvent cutoff radii were set to 12 and 9.75 Å, respectively, whereas the solute−solute atom−atom interactions were calculated at any distance of the ion pair.

With the RESP charges, the FEP calculations were repeated for the $SerH^+\cdots Cl^-$ system. This second series became necessary because the net free energy change with the CHELPG set was about 0.8 kcal/mol after completing a 360° rotation of the $-NH_3^+$ group. This error is known as the hysteresis of the calculation, which should ideally vanish, and, in fact, it was within the calculated standard deviation of the closed perturbation circle for dopamine[2d] and norepinephrine.[3a] The third MC simulation utilized the RESP atomic charge set for the "cation only" model. Long-range electrostatic corrections were calculated by means of the IEF-PCM procedure. Since the solute−solvent cutoff was set to 12 Å, solute−solvent interactions beyond this limit were calculated as corrections. Spheres with radii of 12 Å were formed around each solute atom, and their overlapping volume created the cavity to be used in IEF-PCM/B3LYP/6-31G* single-point calculations. By comparing the results obtained with the two charge sets, the effect of the selected

partial charge model can be investigated. Analogously, from the RESP calculations for the single cation and the ion pair, the counterion effect on relative solvation free energies for the different conformers can be evaluated.

Since the derived charge sets reflect the in-solution geometries and the polarization of the solute by the solvent, the relative internal energy was calculated also from the polarized solute model, thus from IEF-PCM/B3LYP/6-31G* calculations, and the relative total free energy of the protonated serotonin conformers on the basis of Monte Carlo simulations is

$$\Delta G_{tot} = \Delta E^{s}_{int}(\mathrm{PCM}) + \Delta G_{solv}(\mathrm{MC}) \qquad (4)$$

Conformational free energy differences (without the frequency dependent corrections), calculated according to eq 4, have been compared for the three MC models. The structure and some peculiarities of the first hydration shell of the different conformers have been characterized by utilizing radial distribution functions (rdfs) and pair-energy distribution functions (pedfs).

For investigating the interaction of the $SerH^+$ ligand and a model for the 5-HT2A receptor, flexible docking after a short molecular dynamics study was performed. A recently developed muscarinic-1 receptor model has been exploited,[28] based on the rhodopsin structure[7] as a template. On the basis of the correspondence of the residues for the muscarinic-1 and 5-HT2A receptors,[6b] 16−24 amino acids were switched in the middle third of each of the seven transmembrane α-helices. These altogether 150 amino acid side chains may surround the binding cavity or are at the corresponding depth of each helix. Based on studies by Roth et al.[29] and Almaula et al.,[30] the $-NH_3^+$ group was oriented toward the Asp 3.32 (residue 155) and Ser 3.36 (residue 159) side chains of the hypothesized binding cavity in the starting arrangement. The indole part of serotonin pointed toward different aromatic side chains including Phe 5.44, 5.47, 5.48, 6.51, 6.52, and 7.38 (240, 243, 244, 339, 340, and 365), Trp 6.48 and 7.40 (336 and 367), and Tyr 7.43 (370). As mentioned above, each gauche and trans $SerH^+$ conformers have a mirror image isomer with equal internal energy. Since the cavity has, however, a given stereochemistry, the elements of the image pairs would interact with the receptor with different energies. For this reason, the mirror image pairs of protonated serotonin in the G1, G2, and T conformations were placed into the cavity. This resulted in small differences for the interaction of the Asp 3.32 carboxylate and the cationic head of the ligand, but the indole part interacted with different residues from TM V, VI, and VII. The docking studies were performed by the aid of the Sybyl 6.91 software[31] and using the Tripos force field. For the receptor, the all-atom Kollman charge set of Sybyl was utilized, whereas the solute charges were accepted from our in-solution fitted CHELPG set. After removing the poor interactions for the receptor···ligand complex in a pre-energy minimization, a 10 ps long gas-phase molecular dynamics calculation was carried out with each ligand conformations. The Sybyl molecular dynamics module was used in a gas-phase N*VT* ensemble at $T = 310$ K. Solvent effects were implicitly considered in the distance-dependent dielectric approximation of the form $\epsilon = 4r$. The nonbonded cutoff was set to 8 Å. The 10 ps simulation length was supposed to be long enough for a possible change of the ligand conformation and rotation of involved receptor side chains into a more preferable position without destroying the basic structure of the receptor model. The energies of the structures with the smallest potential energy in the 5−10 ps interval as well as the structures obtained after 10 ps MD simulations were minimized. The interaction energy (EI) between the receptor and the ligand was calculated for these minimized structures as

$$\mathrm{EI} = E(\mathrm{add}) - E(\mathrm{rec,add}) - E(\mathrm{lig,add}) \qquad (5)$$

where E(rec,add) and E(lig,add) are the energies of receptor and ligand, respectively, in the optimized adduct. The ligand distortion energy, E(lig,dist), was calculated as E(lig,add) − E(lig,opt), where E(lig,opt) derived from a molecular mechanics optimization with the Tripos force field and CHELPG charges from the present study. Structures and relative energies of the isolated ligands were also considered with the MMFF94 force field.[32] Taking the receptor structure from the adduct after 10 ps MD and minimization, the optimized ligand was placed into the binding cavity at O•• •N distances of 4, 5, and 7 Å for the Asp155 carboxylate oxygen and the $SerH^+$ protonated nitrogen. The indole site was oriented toward the Phe, Trp, and Tyr side chains in TM V, VI, and VII. By performing docking studies from these starting arrangements, 18 further receptor−ligand binding modes were identified. In the absence of the knowledge of the absolute energy minimum of the receptor (whose determination is practically impossible), relative interaction energies and ligand distortion energies may provide qualitative information about the favorable binding mode of protonated serotonin.

III. Results and Discussion

A. Gas-Phase Results. A systematic conformational analysis of all degrees of freedom of protonated serotonin has been carried out in vacuo at the B3LYP/6-31G* level. To explore the conformational space of the indole OH group, the flexible scan of the $H_5O_5C_5C_6$ (φ_4) dihedral angle has been carried out for G1, G2, and T (Scheme 1). Two conformational minima have been found at $\varphi_4 \approx 0°$ and 180° (Figure 1) with the lower barrier joining them about $\varphi_4 \approx 90°$. The local minimum about $\varphi_4 \approx 180°$ is invariably higher than that about $\varphi_4 \approx 0°$ (by 1.2, 1.8, and 2.2 kcal/mol for G1, T, and G2, respectively). Thus all the subsequent calculations took $\varphi_4 \approx 0°$ as a starting conformation.

In accord with our earlier studies on neurotransmitters, the potential energy surface (displayed in Figure 2) was calculated in the gas phase by changing the $C_2C_3C_\beta C_\alpha$ (φ_1) and $C_3C_\beta C_\alpha N$ (φ_2) torsion angles at the B3LYP/6-31G* level. Three local minima, G1, G2, and T, were identified with the TS1, TS2, and TS3 transitions states connecting two neighboring minima when the φ_2 torsion angle changes between 0° and 360° and $0° \le \varphi_1 \le 180°$.

The B3LYP/6-31G* energies for the G1 and T local energy minima relative to the G2 conformer are 0.8 and 6.0 kcal/mol, respectively (Table 1). High barriers, ranging from

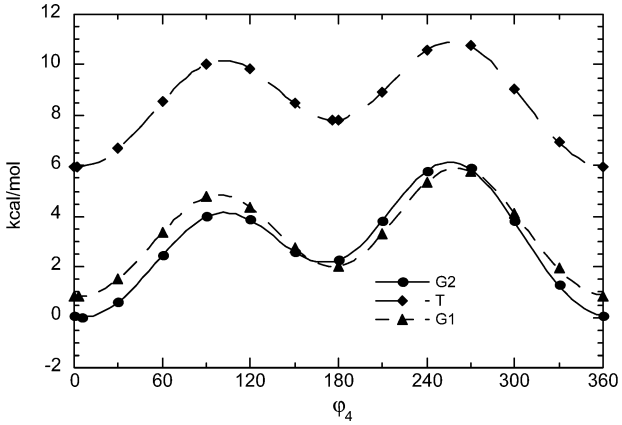

Figure 1. B3LYP/6-31G* potential energy profiles in vacuo for the rotation about $H_5O_5C_5C_6$ (φ_4) for the three main conformers.

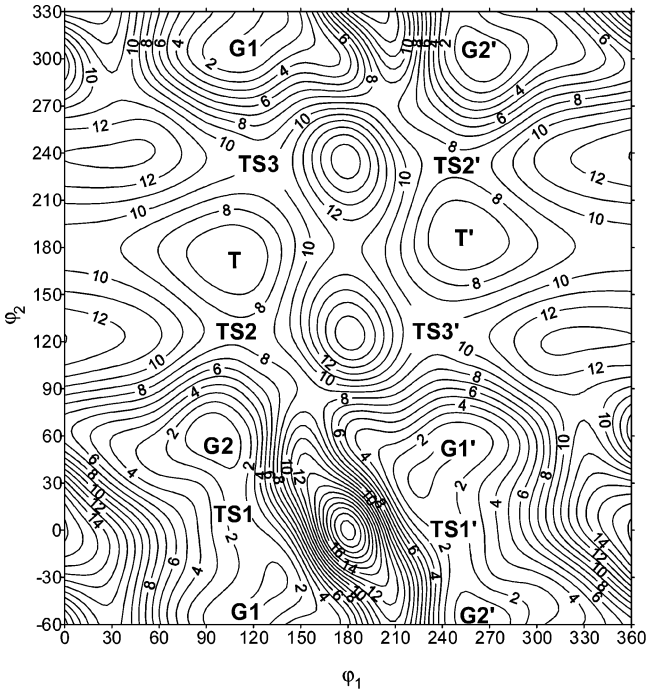

Figure 2. B3LYP/6-31G* potential energy surface in vacuo for the rotation about $C_2C_3C_\beta C_\alpha$ (φ_1) and $C_3C_\beta C_\alpha N$ (φ_2) with the main stationary points indicated.

Table 1. B3LYP Relative Energies (kcal/mol) at Optimized Geometries for Protonated Serotonin in the Gas Phase

	6-31G*	6-311++G**
G2	0[a]	0[b]
TS2 (G2→T)	8.25	7.68
T	5.97	5.62
TS3 (T→G1)	10.15	9.18
G1	0.84	0.66
TS1 (G1→G2)	1.65	1.94

[a] Reference energy (hartrees): −573.389277. [b] Reference energy (hartrees): −573.553883.

9.5 (φ_1=0°, φ_2=180°) to 11.2 kcal/mol (φ_1 = 180°, φ_2 = 180°), hinder the rotation about the C_3-C_β axis. Conversely, a favorable interconversion path with rotation about the $C_\beta-C_\alpha$ axis lies along the $\varphi_1 \approx \pm 120°$ regions.[2] (Hereafter only the path in the $\varphi_1 \approx 120°$ region has been considered, unless

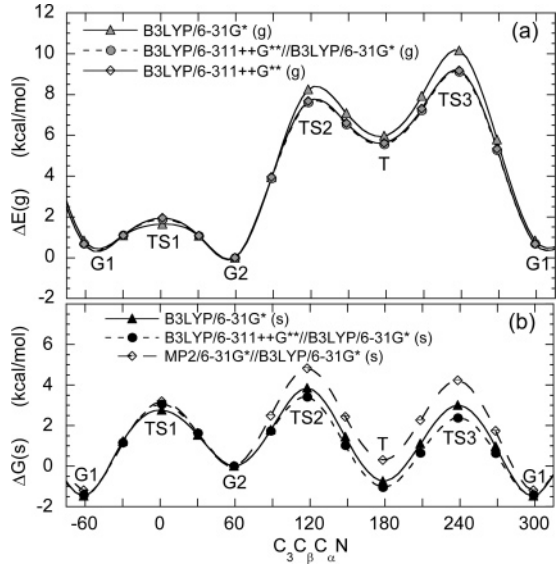

Figure 3. Profiles (kcal/mol) for the rotation about the $C_\beta-C_\alpha$ axis in protonated serotonin of the potential energy in the gas phase (a) (g, empty markers) and of the IEF-PCM free energy in aqueous solution (b) (s, solid markers). Solid lines = optimized structures; dashed lines = single point calculations at the B3LYP/6-311++G** or MP2/6-31G* level on the B3LYP/6-31G* structures.

otherwise specified (stationary points in the $\varphi_1 \approx -120°$ region are marked with a prime).) The TS1 transition state (ΔE = 1.6 kcal/mol) separates G1 and G2, with barriers of 0.8 kcal/mol for the G1 to G2 transformation. This transition state is, however, much lower in energy than T (ΔE = 6.0 kcal/mol). The TS2 and TS3 transition state energies between T/G2 and T/G1 are 8.3 and 10.2 kcal/mol, respectively, providing barriers of 2.3 and 4.2 kcal/mol for the T to G2 and T to G1 rotations, respectively. Finally, the G1 to T barrier turns out to be 9.3 kcal/mol, as can be derived from Table 1 and Figure 3a.

From the point of view of a conformational analysis, determination of the potential energy as a function of the torsion angles is the most critical task. Due to the importance of diffuse functions when calculating relative energies with DFT,[33] B3LYP/6-311++G** optimizations for the local energy minima and TS have been carried out starting from the corresponding B3LYP/6-31G* structures. Figure 3a shows the energy profiles as a function of the $\varphi_2 = C_3C_\beta C_\alpha N$ torsion angle at the B3LYP/6-31G*, B3LYP/6-311++G**// B3LYP/6-31G*, and B3LYP/6-311++G** levels in vacuo. The rotational curves, with a very similar 3-fold maximum−minimum pattern separated by about 120°, show limited variations in the barrier heights among the various descriptions. For the TS3 barrier at φ_2 = 240°, the values in kcal/mol with the 6-31G*/6-311++G** basis sets are 9.3/8.5 (G1 to T) and 4.2/3.6 (T to G1), respectively. For the TS2 barrier at φ_2 = 120°, the relevant values in kcal/mol are 2.3/2.1 (T to G2) and 8.3/7.7 (G2 to T), respectively. Finally, the TS1 barrier in kcal/mol at φ_2 = 0° (or 360°) is 1.6/1.9 (G2 to G1) and 0.8/1.3 (G1 to G2) at the two levels (Table 1).

The basis set effect is almost insignificant on the geometries, whereas relative energies change by 0.2−1.0 kcal/mol, primarily for the TS structures. The larger basis set

generally decreases the relative energies with the exception of the TS1 conformer energy. Nonetheless, Table 1 suggests unequivocally that the G2 structure is the lowest energy conformer of the six ones, and the other gauche structure is higher in energy by less than 1 kcal/mol. The trans, extended side-chain T structure has a relative energy of about 6 kcal/mol in the gas phase. The TS1 barrier separating G1 and G2 is relatively small, less than 2 kcal/mol. TS2 and TS3 barriers separating the T structure from any gauche conformers are, however, as high as 8 kcal/mol (Figure 3a).

The optimized values of the $C_2C_3C_\beta C_\alpha$ and $C_3C_\beta C_\alpha N$ torsion angles calculated at the two levels (reported in Table S1 in the Supporting Information) differ moderately, and the values are close to the classical torsion angles in a staggered or an eclipsed ethane conformer. Variations of the corresponding torsion angles at the different levels are generally less than 5°.

B3LYP/6-31G* optimizations were followed by frequency analysis, which confirmed the extreme point character of the six structures on the PES. Some selected normal frequencies are provided in the Supporting Information (Table S2), where the calculated IR spectra for cationic serotonin in the gas phase are also available (Figure S1). Similarly to our previous results for protonated gas-phase norepinephrine,[3a] the lowest three frequencies correspond to the $C_2C_3C_\beta C_\alpha$ torsion, the $C_3C_\beta C_\alpha$ bending, and the $C_3C_\beta C_\alpha N$ torsion, respectively. Although we calculated norepinephrine frequencies at the HF/6-31G* level, the B3LYP/6-31G* values are similar, and mainly the separation of the calculated frequencies resemble in the two calculations. This similarity suggests that low frequencies and their distribution are close to each other in the protonated, 2(aromatic-ring)-substituted ethylamines.

B. In-Solution Results. *1. Continuum Solvent.* In the aforementioned norepinephrine study[3a] we faced two problems when in-solution calculations were performed. We used gas-phase optimized geometries and utilized atomic charge parameters derived from these calculations for in-solution Monte Carlo simulations. Both problems are overcome in the present theoretical approach, which requires, however, much larger computational effort.

IEF-PCM/B3LYP/6-31G* geometry optimizations in aqueous solution led to small changes in the torsion angles as compared to the gas-phase structure. Bond lengths and angles vary also upon solvation, but the energy effect concomitant to a bond increase or shortening is considerably larger than a change of a few degrees in the torsion angles. In a recent study[20a] we found that the geometry distortion upon solvation, calculated at the PCM/B3LYP/6-31G* level, causes an increase in the internal energy (calculated in the gas phase at the in-solution optimal geometry) up to a few tenths of a kcal/mol for small molecules. This energy change is not negligible in the case of a conformational equilibrium for components in nearly equal concentration.

In-solution geometry optimizations are more important, however, to derive relevant net atomic charges to be applied in the 12-6-1 effective pair potential utilized in Monte Carlo simulations. As discussed earlier,[20] the BOSS program calculates the interaction energy of the solution elements by the implication that the atomic charge parameters represent a polarized electron distribution existing in the solution. The charge parameters for the TIP4P water model were developed accordingly.[26] In prior applications, atomic charges for the solute were derived based on a fit of the gas-phase HF/6-31G* electrostatic potential by Orozco et al.[34] The argument supporting the use of this procedure was that the HF/6-31G* basis set overestimates the gas-phase dipole moments by about 20%, so a fit to the corresponding molecular electrostatic potential could implicitly account for the polarized charge distribution of the solute in solution. This procedure, however, may not work well for every kind of solute molecules and does not account for the different charge distributions in different solvents. Conversely, the present approach is applicable for any molecule in any solvent.

The relative free energies for the different protonated serotonin conformers, as calculated based on IEF-PCM/B3LYP/6-31G* geometry optimizations as well as from IEF-PCM/B3LYP/6-311++G** and IEF-PCM/MP2/6-31G* single point calculations at the IEF-PCM/B3LYP/6-31G* optimized geometries, are compared in Figure 3b.

The gas-phase and in-solution curves in Figure 3 differ substantially. Although both types of curves show three maxima and minima, the barrier heights and stabilities of the local minima are quite different. In the gas phase, G2 is the most stable structure, and the T conformer corresponds to a high-energy local minimum. The barrier heights corresponding to the TSs occurring at $C_3C_\beta C_\alpha N$ values of around 120° and 240° are 8−10 kcal/mol. In contrast, IEF-PCM/B3LYP/6-31G* calculations predict the G1 structure to be the lowest free energy one, while T is higher in free energy only by 0.7 kcal/mol. The G2 relative free energy is 1.5 kcal/mol. The G1 to G2 barrier, TS1, increased to 4.3 kcal/mol, on the contrary the G2 to T (TS2) and T to G1 (TS3) barriers decreased to 3.8 and 3.7 kcal/mol, respectively. Overall, the in-solution relative conformational free energy curve shows a 3-fold potential with three similar energy minima in a 1.5 kcal/mol range, and the barriers are in a 3−4.5 kcal/mol range. Similar conclusions are obtained from the analyses of the other two in-solution potentials from single point calculations. The MP2/6-31G*//B3LYP/6-31G* results in the $60° < \varphi_2 < 300°$ region turn out to be somewhat less favorable than the B3LYP ones, probably because of the decrease of the dispersion interaction for the extended T form, not accounted for by B3LYP. A stabilization of about 1 kcal/mol for the trans conformer relative to a gauche one for 2-phenylethylamines seems to be a general feature at the B3LYP/6-31G* level in comparison to the MP2/6-31G* level, as we found either for protonated dopamine[2d] and norepinephrine[3a] or for neutral and zwitterionic tyramine (2-(4OH-phenyl)ethylamine) and dopamine in a recent study.[2g]

Using the IEF-PCM/B3LYP/6-31G* frequencies, the IR spectra of protonated serotonin have been calculated for the G1, G2, and T conformations (see Figure S2 in the Supporting Information). Some selected frequencies are provided in Table S3 in the Supporting Information. Comparison of the normal frequencies in aqueous solution with those in vacuo (Table S2) shows a remarkable lowering of the $C_3C_\beta C_\alpha N$ torsion frequency for the G2 conformer. From

Table 2. Unscaled Free Energy Correction Terms (kcal/mol) at the B3LYP/6-31G* Level Relative to the G2 Conformer in Vacuo and in Solution at $T = 310$ K and $p = 1$ atm

vacuo	ΔZPE	$\Delta(H(T)-\text{ZPE})$	$-T\Delta S_{tot}(T)$	$\Delta G_{th}(T)$
TS2	−0.26	−0.31	0.55	−0.02
T	−0.19	0.24	−0.86	−0.81
TS3	−0.29	−0.26	0.02	−0.53
G1	−0.13	0.04	−0.30	−0.39
TS1	−0.05	−0.38	1.16	0.73
water	**ΔZPE**	$\Delta(H(T)-\text{ZPE})$	$-T\Delta S_{tot}(T)$	$\Delta G_{th}(T)$
TS2	0.02	−0.49	1.29	0.83
T	0.13	0.03	0.12	0.28
TS3	0.08	−0.49	1.27	0.86
G1	0.17	−0.09	0.46	0.54
TS1	0.07	−0.51	1.48	1.04

Figure 3, the barriers are high enough to consider the motion as a vibration instead of a hindered rotation. The above finding has an important effect on the calculated relative thermal free energy contribution, $\Delta G_{th}(T)$, as defined in eq 1 (Table 2). Since the molecular weight is constant, and the moments of inertia change generally only a little for the substituted ethylamine conformers,[3a] the main contribution to $\Delta G_{th}(T)$ comes from the $T\Delta S_{vibr}(T)$ term for the local energy minimum structures. Within this term, the largest contributions come from the lowest frequency vibrations, which are, however, the least accurate and hence also contribute the largest error to the entropy. Comparison of the in vacuo and in-water $\Delta G_{th}(T)$ values confirm our previous finding. Whereas the in vacuo thermal corrections relative to the G2 conformers are negative values (with the exception of the +0.7 kcal/mol for the TS1 transition state), all $\Delta G_{th}(T)$ values become positive in solution.

The curves in Figure 3 do not contain thermal corrections. The use of the rigid rotator-harmonic oscillator model must be approximate even in the gas phase and probably even less adequate for solutes. Considering, however, that $\Delta G_{th}(T)$ refers to conformers of the same species, a remarkable cancellation error may be expected. By considering these correction terms, the G2-G1 and the T-G2 free energy separation decreases by 0.5 and 0.3 kcal/mol, respectively, providing total free energies for the G2 and T forms relative to the G1 form of 1.0 and 0.4 kcal/mol, respectively.

2. Monte Carlo Simulations. Two different charge sets, RESP and CHELPG, were used in MC simulations for each rotamer as stated in the Calculation section. They are visually compared in Figure S3, while a detailed numerical summary is provided in Tables S4 and S5 in the Supporting Information. The general shape of the two charge-alteration curves is similar. The largest difference in the *shape* is on the left-hand side of the plots referring to the C_3 to C_7 atoms, all belonging to the aromatic ring system (Scheme 1). RESP assigns to the C_2, C_7, and C_6 atoms nearly equal atomic charges (∼ −0.2 charge units). For these atoms the CHELPG charges are within ∼0.3 charge units. In contrast, the RESP change amounts to ∼0.1 units for C_9 and C_8, which are almost constant from the CHELPG fit. Trends are similar for the C_6 to H_{g1} atoms. The CHELPG charges differ considerably for the amine nitrogen, N_{am}, and for the g2 gauche proton in the $-NH_3^+$ group as a function of the conformation. The conformation dependence for these atoms is smaller at the RESP level. Considering the numerical values for specific atoms, the largest difference was found for the pyrrole nitrogen, N_1, and C_5 to N_{am} atoms. Although the O_5 charge is similar in both sets, the C_5-O bond is more polarized with the CHELPG fit than with the RESP one.

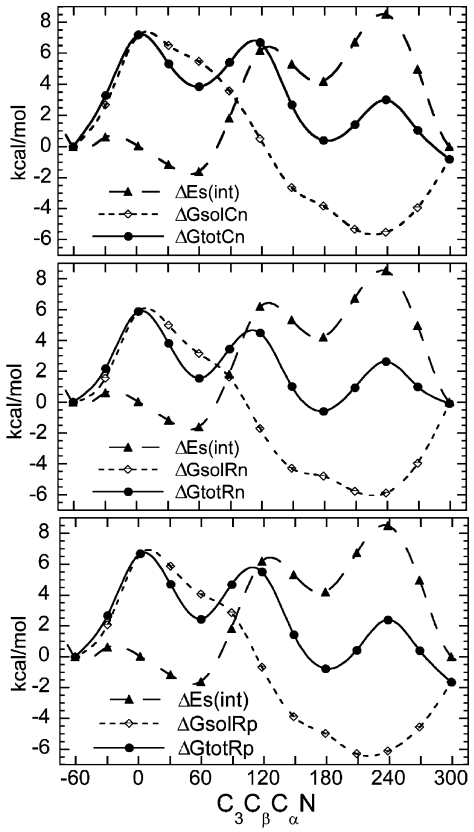

Figure 4. Conformational free energy differences compared using the three MC models. ΔE s(int) stands for ΔE^{s}_{int} (IEF-PCM/B3LYP/6-31G*) of eq 3a, ΔG_{sol}Cn (top) and ΔG_{sol}Rn (middle) stand for ΔG_{solv} in the $SerH^+\cdots Cl^-$ system with the CHELPG and RESP charges, respectively, while ΔG_{sol}Rp (bottom) stands for the ΔG_{solv} values in the $SerH^+$ system with the RESP charges. For ΔG_{tot}, the sum of ΔE^{s}_{int} (IEF-PCM) and ΔG_{solv}, the same notation as for ΔG_{solv} is used.

The largest difference in polarity was found for the $C_\alpha-N_{am}$ bond. The RESP polarity is ∼0.3 units, whereas the CHELPG value amounts to 0.7 units. Overall, the CHELPG as compared to the RESP fit results in a more polar charge distribution for protonated serotonin. This finding is consistent with the calculated ΔG_{solv} values in Figure 4.

Figure 4a−c shows the internal energy of the polarized solute, ΔE^{s}_{int} (IEF-PCM/B3LYP/6-31G*), ΔG_{solv}, and the total relative free energy in solution, ΔG_{tot}, computed as a summation of ΔE^{s}_{int} (IEF-PCM) and ΔG_{solv} for the three MC models studied. The ΔE^{s}_{int} (IEF-PCM) curve is similar to the in vacuo, nonsymmetric, 3-fold B3LYP/6-31G* potential in Figure 3a. The polarization of the solute in solution leads, however, to a deeper minimum at φ_2 ($C_3C_\beta C_\alpha N$) about 60° (G2 conformer), and the relative internal energy for the T conformer (φ_2 about 180°) is

Table 3. Total Relative Free Energies for the Protonated Serotonin Conformers Optimized at the IEF-PCM/B3LYP/6-31G* Level in Aqueous Solution

	continuum model (IEF-PCM) B3LYP/6-31G*	Monte Carlo		
		CHELPG	RESP	RESP (cation)
G1	0	0	0	0
TS1	4.2	7.2 ± 0.2	5.9 ± 0.1	6.7 ± 0.1
G2	1.5	3.9 ± 0.3	1.5 ± 0.3	2.4 ± 0.2
TS2	5.3	6.7 ± 0.4	4.5 ± 0.4	5.5 ± 0.2
T	0.7	0.4 ± 0.4	−0.6 ± 0.4	−0.8 ± 0.3
TS3	4.5	3.0 ± 0.4	2.6 ± 0.4	2.4 ± 0.3
	continuum model (IEF-PCM) MP2/6-31G*//B3LYP/6-31G*	Monte Carlo		
		CHELPG	RESP	RESP (cation)
G1	0	0	0	0
TS1	4.4	6.9 ± 0.2	5.6 ± 0.1	6.4 ± 0.1
G2	1.2	3.4 ± 0.3	1.1 ± 0.3	2.0 ± 0.2
TS2	6.0	7.3 ± 0.4	5.1 ± 0.4	6.1 ± 0.2
T	1.5	1.0 ± 0.4	0 ± 0.4	−0.2 ± 0.3
TS3	5.4	3.8 ± 0.4	3.4 ± 0.4	3.2 ± 0.3

reduced from 6.0 to 4.2 kcal/mol. The two TS occurring at φ_2 values of about 120° (TS2) and 240° (TS3) are less high by ∼2 kcal/mol each.

The ΔG_{solv} curves are similar in shape but different in amplitudes. Each of them have a maximum at $\varphi_2 = 0°$ (TS1) with relative values of 7.2, 5.9, and 6.7 kcal/mol, respectively, for a, b, and c simulations. The minima are in the $\varphi_2 = 210-240°$ range with −5.5, −5.9, and −6.3 kcal/mol, respectively, for a, b, and c. Thus ΔE^{s}_{int} (IEF-PCM) and ΔG_{solv} curves run oppositely. Slightly negative relative internal energies are combined with largely positive ΔG_{solv} values in the φ_2 range of −60° to 60°. In contrast, large positive ΔE^{s}_{int} (IEF-PCM) contributions are combined with strongly negative ΔG_{solv} terms for $\varphi_2 = 180°$ to 300°. It is important to remark that the solvation curve in Monte Carlo simulations is not sensitive to internal energy changes, thus it does not show a periodicity for local energy minimum and TS structures. Rather it depends on the relatively buried or solvation-exposed character of the $-NH_3^+$ group. Accordingly, ΔG_{solv} is positive in the $C_3C_\beta C_\alpha N$ torsion angle range of −60° to 60°, where the protonated group leans above the ring system and is the most negative in the $C_3C_\beta C_\alpha N = 180-240°$ range with an extended, nearly trans side-chain conformation. The solvation term reminds of a sine curve, irrespective of the parametrization or whether the chloride counterion has been included or not.

As a result, the $\Delta G_{tot} = \Delta E^{s}_{int}$(IEF-PCM) + ΔG_{solv}(MC) total relative free energy curve corresponds to a moderately nonsymmetric 3-fold potential in the entire 360° rotation range. The overall conclusion is that the three Monte Carlo solvation models as well as the IEF-PCM/B3LYP/6-31G* continuum solvent model are qualitatively equivalent but provide results differing in fine details. These details are important, however, in calculating the equilibrium conformer composition. Table 3 summarizes the relative free energies without considering thermal corrections. In addition, in the bottom part of the table, results based on IEF-PCM/MP2/6-31G*//IEF-PCM/B3LYP/6-31G* calculations are reported. With respect to the remarkable shift of the relative free energy for the T conformer at the two levels, the MP2 results deserve special attention.

All calculations agree that the G2 gauche conformer is of high relative energy and can be present in the equilibrium composition with only a small fraction. If ΔE^{s}_{int} is calculated on the basis of the IEF-PCM/B3LYP/6-31G* values, the corresponding continuum solvent results for the total relative free energies and the CHELPG MC predicts the G1 gauche conformer to be the most stable, but the relative CHELPG value of 0.4 ± 0.4 for the T trans conformation allows an almost equal G1 and T population. The RESP parametrization favors the T form both with and without considering the counterion. If the relative thermal corrections from Table 2 are also considered, all Monte Carlo models predict the trans conformation as the prevailing one in aqueous solution, whereas the IEF-PCM model still prefer the G1 form over the T conformation by 0.5 kcal/mol.

A different composition is predicted, however, on the basis of IEF-PCM/MP2/6-31G*//IEF-PCM/B3LYP/6-31G* calculations. At that level, the relative free energies predict a 1.5 kcal/mol destabilization of the T form as compared to the 0.7 kcal/mol gap obtained from the B3LYP/6-31G* results. If ΔE^{s}_{int} is calculated using the MP2 internal energies of the in-solution polarized solute, the subsequent CHELPG/MC predicts the prevalence of the G1 form in solution, in accord with the IEF-PCM calculations. The mean ΔG_{tot} value of T calculated with the RESP parametrization for the ion pair allows a nearly equal population for the G1 and T conformers in aqueous solution. The inclusion of thermal corrections leads to ΔG_{tot} values of 1.2, 0.7 ± 0.4, and −0.3 ± 0.4 kcal/mol for the T conformer at the IEF-PCM, CHELPG/MC, and RESP/MC levels, respectively. The RESP(cation) ΔG_{tot} value with thermal corrections for T is −0.5 ± 0.3 kcal/mol, favoring the T conformer over G1. The solution structure analysis (see next section) has pointed out, however, that the solvation of the $SerH^+$ cation only may exaggerate the stabilization of the trans conformer relative to the gauche $SerH^+$ conformations.

In summary, the theoretical models are sensitive to the

selected method (continuum or explicit solvent), to the theoretical level in continuum calculations (MP2 or B3LYP), and to the charge parametrization within the MC simulations. The predicted relative free energies for the conformers allow a sensitive equilibrium between the extended trans and the more globular gauche conformers in aqueous solution. In the absence of experimental results, the theoretical prediction cannot be controlled at present. The significant shift in the trans relative energy at the MP2/6-31G* vs B3LYP/6-31G* levels for 2-phenylethylamines supports, however, the MP2/6-31G* internal energies in comparison with the B3LYP/6-31G* values.[35] By calculating a trans−gauche energy separation of about 1 kcal/mol at the MP2/6-31G* level for neutral tyramine, Melandri and Maris[38] found a good accord between the theoretical and experimental compositions derived on the basis of the free-jet microwave spectrum. In contrast, B3LYP/6-31G* geometry optimizations lead to about equal energies for these conformers, whereas the conformer composition calculated on the basis of MP2/6-31G*//B3LYP/6-31G* results agree fairly well with the experimental one.[2g]

A comparison with earlier calculations shows that the conformational preference for 2-substituted ethylamines in aqueous solutions at pH = 7 is a resultant of a subtle balance between internal and solvation free energies. Histamine, dopamine, norepinephrine, and serotonin are protonated at their amine groups at least 92% at pH = 7.4.[3a] Protonated histamine prefers a gauche side chain ($C_{ring}C_\beta C_\alpha N$) conformation with an intramolecular N−H···N hydrogen bond as predicted theoretically[1c] and found experimentally.[1g] On the basis of Solmajer et al.[39] experimental study, the protonated dopamine favors a $C_{ring}C_\beta C_\alpha N$ gauche conformation at pH = 7, whereas these authors found the $C_{ring}C_\beta C_\alpha N$ trans arrangement as the most preferred conformation under similar conditions for norepinephrine. Our previous theoretical results for those systems were at least in qualitative accord with the experimental conformer populations.[2d,3a] All the above results correspond to free energy differences of a few tenths of a kcal/mol for the two most stable conformers. The present sophisticated approach slightly favoring the trans conformer in aqueous solution is in accord with the previous findings.

3. Solution Structure. The $O_{w(ater)}\cdots H(N_{am(monium)})$ radial distribution functions (rdfs) for the trans and gauche hydrogens of the $-NH_3^+$ group in the G1 conformation are compared in Figure 5. As was mentioned in the previous section, the $-NH_3^+$ group leans above the pyrrole ring in the G1 conformer. Since the $-NH_3^+$ group has a staggered conformation relative to the H_2C_α group, the trans hydrogen in the NH_3^+ group is still exposed to favorable solvation, whereas the gauche hydrogens point toward the ring system. This difference is clearly seen on the corresponding rdfs. The g(*R*) peak for $H_{t(rans)}$ is about twice as high as for the $H_{g(auche)}$ atom. The difference means remarkably more localized water solvent molecules around the trans hydrogen than the gauche one. The maximum of the peak occurs at a shorter distance for the trans than for the gauche hydrogen. This means that the favorable $O\cdots H_t$ separation is shorter than the $O\cdots H_g$ distance, which can also be explained by

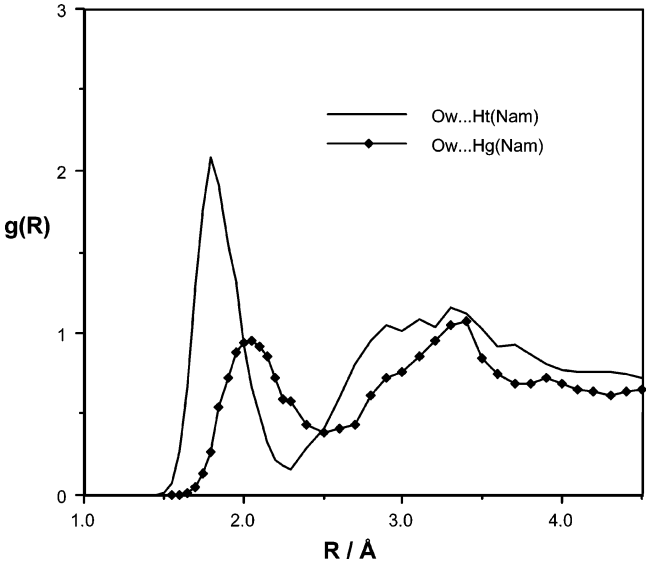

Figure 5. $O_w-H(N_{am})$ radial distribution functions for the trans and the gauche hydrogens of the $-NH_3^+$ group as calculated for the G1 conformer of the $SerH^+$ cation in the $SerH^+\cdots Cl^-$ system. RESP charge parametrization.

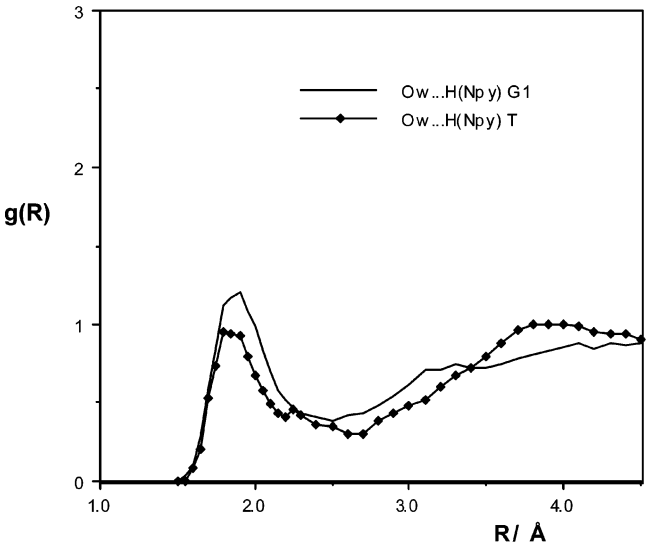

Figure 6. $O_w-H(N_{py})$ radial distribution functions for the G1 and T conformers of the $SerH^+$ cation in the $SerH^+\cdots Cl^-$ system. RESP charge parametrization.

steric effects. The rdf represents, however, only a short-range effect, because the curves run very close to each other for $R > 3.4$ Å. The difference in the hydration of gauche and trans $-NH_3^+$ hydrogens is considerable only for G conformations. In the T structure, the rdfs (not shown) have peak g(*R*) values in the range of 1.36−1.63 at $R = 1.80-1.85$ Å.

The hydration of the pyrrole hydrogen is less sensitive to the side-chain conformation (Figure 6). In fact, the $O_w\cdots H(N_{py(rrole)})$ rdf has a higher g(*R*) peak for the G1 than for the T conformer. A possible explanation is that water molecules are strongly bound to the protonated side chain, which leans above the pyrrole ring in the G1 conformation. As a secondary effect, these water molecules contribute to the hydration of the pyrrole hydrogen. Nonetheless, the peak values are in the range of 1.0−1.2, only slightly exceeding the value of g(*R*) = 1. On the basis of the definition of radial

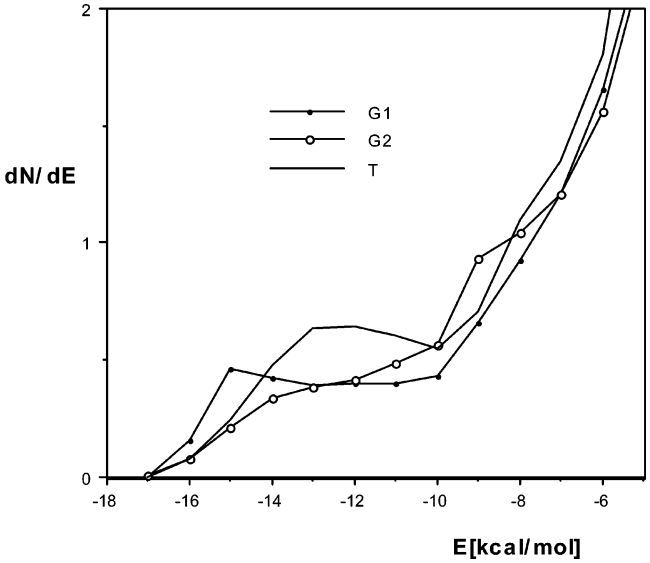

Figure 7. Pair-energy distribution functions for the G1, G2, and T conformers of the $SerH^+$ cation in the absence of the counterion. RESP charge parametrization.

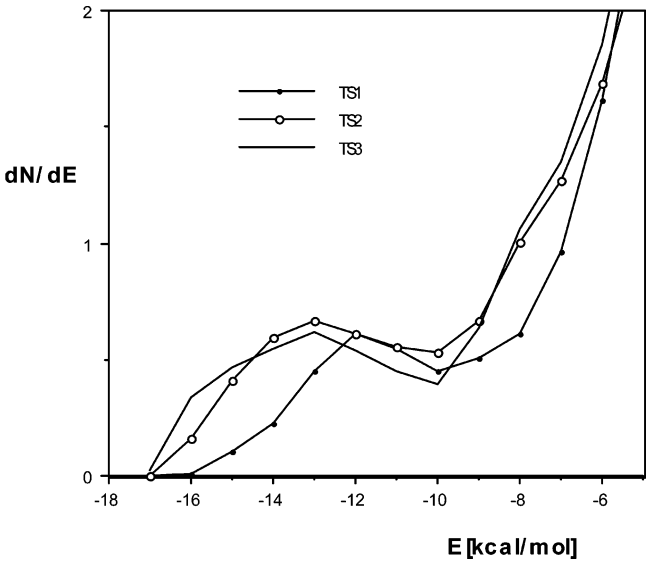

Figure 8. Pair-energy distribution functions for the TS1, TS2, and TS3 transition states of the $SerH^+$ cation in the absence of the counterion. RESP charge parametrization.

distribution functions, this means that the probability of finding a water oxygen at a distance of about 1.9 Å from the pyrrole hydrogen is up the 20% larger than finding a water molecule anywhere in the bulk solvent.

Figures 7 and 8 compare the pair-energy distribution functions for the $SerH^+$ cation (thus for the system without the chloride counterion) calculated with the RESP charges. The pair energy distribution functions (pedfs), dN/dE as a function of E, give the number of water molecules (N) in energy interaction of $E \pm \Delta E$ with the solute, where ΔE was set to 0.5 kcal/mol in the present study. The pedfs in Figure 7 refer to the G1, G2, and T structures with local internal energy minima. Their general trend is essentially similar: all of them start at $E = -17$ kcal/mol. The G1 curve rises more rapidly and is twice as high as the other two at $E = -15$ kcal/mol. It means that the strongest water−solute

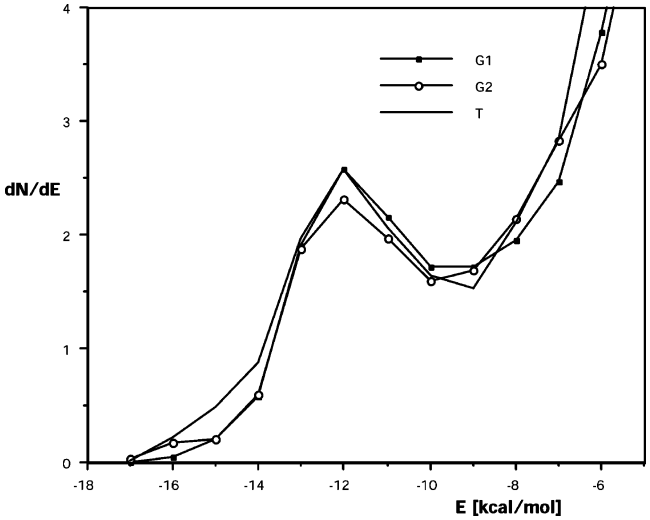

Figure 9. Pair-energy distribution functions for the G1, G2, and T conformers of the $SerH^+$ cation in the $SerH^+\cdots Cl^-$ system. RESP charge parametrization.

interactions are established for a gauche $C_3C_\beta C_\alpha N$ side-chain conformation. However, the G1 pedf does not increase further on until $E = -9$ kca/mol. In contrast, the pedf is highest for the T conformer in the E range of -14 to -10 kcal/mol, which means that T is solvated by the largest number of water molecules with interaction energy of -14 to -10 kcal/mol. Accordingly, this energy range has the largest contribution to the integral of the corresponding pedf, providing the largest N_{HB} value for the trans conformer in a forthcoming table. For less negative E values every pedf rises steeply.

It is interesting to observe that the pedfs for TS structures (Figure 8) do not substantially differ from those for local internal energy minima conformers. Pedfs for TS start also at $E = -17$ kcal/mol and reach a slight maximum in the -17 to -10 kcal/mol interaction range, and after this breaking point the curves sharply increase. Both in Figures 7 and 8, the dN/dE values are around 0.5 in the range of $E = -14$ to -10 kcal/mol. These similarities in the pedf values for TS and local internal energy minimum structures support the explanation given in the previous section that the solvent effect is more determined by the molecular geometry than by the internal energy. A very implicit effect still must be there: the electrostatic solute−solvent interaction energy at a given geometry depends only on atomic charges, and atomic charges were derived by fitting the molecular electrostatic potential, which, however, depends on the internal structure of the solute.

Pedfs for the $SerH^+\cdots Cl^-$ solute system are compared in Figure 9. These pedfs for G1, G2, and T conformers are completely different from those in Figure 7. Although they also start at $E = -17$ kcal/mol, all pedfs have a sharp peak at $E = -12$ kcal/mol and a minimum in the -10 to -9 kcal/mol range. The basic difference of pedfs calculated in the presence or absence of the chloride ion indicates the importance of considering a counterion in the modeling process. Based only on the existence of such a difference, one still could not make a choice. Since, however, under

Table 4. Coordination Numbers (n_{Coo}) and Numbers of Hydrogen Bonds (N_{HB}) in the Presence and Absence of a Chloride Counterion[a]

		$SerH^+\cdots Cl^-$	$SerH^+$
		G1	
n_{Coo}	Cl/H	7.5	
	$H(N_{am})/O^b$	1.1	0.9
	H(O)/O	0.9	1.1
	$H(N_p)/O$	1.1	1.0
N_{HB}		10.9 ($E_{max} = -9$)	2.7 ($E_{max} = -10$)
		G2	
n_{Coo}	Cl/H	7.6	
	$H(N_{am})/O^b$	1.0	1.0
	H(O)/O	1.0	1.0
	$H(N_p)/O$	1.0	1.0
N_{HB}		10.4 ($E_{max} = -9$)	2.5 ($E_{max} = -10$)
		T	
n_{Coo}	Cl/H	7.5	
	$H(N_{am})/O^b$	1.1	1.3
	H(O)/O	1.0	1.0
	$H(N_p)/O$	1.0	1.0
N_{HB}		11.4 ($E_{max} = -9$)	3.2 ($E_{max} = -10$)

[a] For the sake of comparison, all values are relevant to MC simulations with RESP charges; E_{max} in kcal/mol. [b] Average value.

real circumstances the overall system must be neutral, the inclusion of a counterion would provide a more realistic model.

The above conclusion may be, however, only conceptual and may affect only fine details of the simulations. Some solution structure characteristic numbers, compared in Table 4, show small differences for the solute solvation in the presence or absence of the counterion. The chloride by water hydrogen coordination number (Cl/H) hardly changes upon conformational variations in the solute (its calculated value is stably 7.5−7.6).

Only small changes have been computed in the average $H(N_{am})/O_w$ ($H(N_{am})/O$), H(phenolic)/O_w (H(O)/O), and $H(N_{py})/O_w$ ($H(N_p)/O$) coordination numbers for G1 and G2 solute conformers. All these values are 1.0 ± 0.1. The only "large" difference, 0.2 units, was calculated for the $H(N_{am})/O$ coordination number in the T conformation. Since the $C_3\cdots Cl$ distance was set to 12 Å, the distance between the $SerH^+$ and the anion is fairly large in most orientations of the side chain. Nonetheless, the extended side chain, thus the T conformer, can feel the effect of the counterion at a great degree in some arrangements. The decrease of the $H(N_{am})/O$ value of 1.3 for $SerH^+$ to 1.1 in the $SerH^+\cdots Cl^-$ system suggests that the two ionic sites compete in the strong localization of water molecules. In the absence of a chloride ion, $SerH^+$ could localize a larger number of water molecules with its extended side chain. The competition is not obvious for G1 and G2 conformers, where the side chain leans above the ring system in such a position that the hydration is less favorable even in the absence of the counterion.

Numbers of strong hydrogen bonds, N_{HB}, were calculated by the integration of the pedfs up to the first minima or until the ends of the plateaus. The upper energy limits are indicated in parentheses in Table 4. If $E_{max} = -9$ kcal/mol is allowed for the $SerH^+$ systems as well, the computed numbers are 3.3, 3.4, and 3.9 for G1, G2, and T conformers, respectively. Subtracting these values from the N_{HB} values for $SerH^+\cdots Cl^-$, nearly the corresponding Cl/H are obtained. Thus, the large difference in the N_{HB} numbers is related to the hydrogen bonds connected to the chloride ion. Since this difference is either equal to the Cl/H coordination numbers within the rounding error (G1 and T) or slightly less than the Cl/H value, one can interpret the result in this way: all hydrogens in the first shell (about 7.5) are H-bonded to the chloride with the G1 and T conformations, or about 7 hydrogen bonds are there with the G2 solute rotamer. The number of hydrogen bonds according to this calculation is just 3.3−3.4 units for G conformers, and N_{HB} is slightly larger for the more favorably hydrated T conformer. Using the more severe integration limit of $E = -10$ kcal/mol, 2.5−2.7 H-bonds are obtained for G conformers and 3.2 for the T form. The difference in the number of the hydrogen bonds for G and T conformers is maintained in the two calculations.

The N_{HB} numbers in Table 4 were calculated by an integration till $E = -9$ kcal/mol at most. The comparison of the values for the two models indicates the chloride as hydrated by 7−8 water molecules (almost all of them) H-bonded to it. There are about three *very* strong hydrogen bonds ($E = -17$ to -9 kcal/mol) to the protonated serotonin solute, whose primary location sites have been identified here, in accord with previous studies,[1c,2d,3a] in the first hydration shell of the $-NH_3^+$ group. There are, however, at least two additional hydrogen-bonding sites in the molecule: the phenolic (aromatic) OH and the pyrrole NH site. Both sites were studied by us previously: the phenolic $OH\cdots O_w$[40] and pyrrole $NH\cdots O_w$[41] hydrogen bond energies were found to be less favorable than those involving the ammonium group (i.e. less negative than about −9 kcal/mol). The pedfs are monotonically increasing after this limit, while no separate and resolved maximum−minimum character can be seen for these interactions, because solute−water interaction energies with water molecules in the second hydration shell appear also in the indicated energy range. Nonetheless, the clear shoulder for G2 and the less obvious one for T (see Figure 7), located in the energy range −10 to −7 kcal/mol, are assigned to the nonionic $H\cdots O_w$ interactions including the two mentioned sites.

C. Docking Studies. The 2-(aromatic ring) substituted ethylamine neurotransmitters (histamine, dopamine, norepinephrine, epinephrine, and serotonin) may have their biochemical specificities simply due to the chemical difference in the aromatic ring, ring or side-chain substituents (norepinephrine and epinephrine have a 2-OH group, as well), different protonation abilities of the amine group (this group is an N-methyl secondary amine group for epinephrine) or due to the differences in the favorable conformation(s) of the molecules. This latter may also be a consequence of the chemical character of the 2-substituent.

In Figure 10, our optimized structures for dopamine and norepinephrine (from previous studies) and for serotonin are superimposed in the three main side-chain conformations. In the top part of the figure, the catechol ring and the phenol substructures of the 5-OH indole system are superimposed, while in the bottom part the side chains. Whereas the

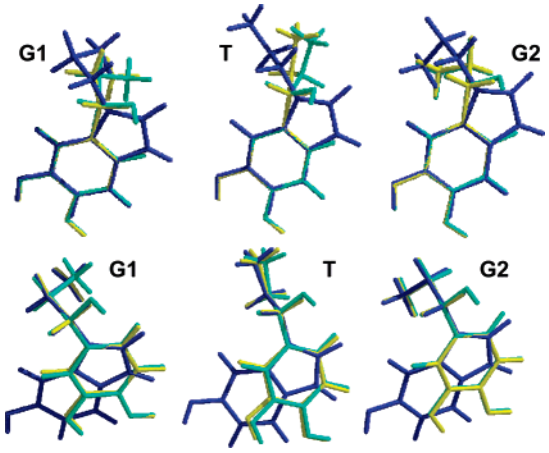

Figure 10. Optimized structures for protonated serotonin (blue) in the three main side-chain conformations, superimposed to those for dopamine (yellow) and norepinephrine (cyan) derived from our previous studies, on: (top) catechol rings and the phenol substructure of 5-OH indole; (bottom) $C_2C_3C_\beta C_\alpha$.

dopamine and norepinephrine molecules, differing only in the 2-OH group, are in both cases very well superimposable, superimposition of serotonin to these molecules fails. The superimposition is better for the side-chain fit, indicating that the three molecules have similar stable conformations with G1, T, and G2 side-chain arrangements. Thus we conclude that the neurotransmitter specificity for these molecules lies in the difference of the chemical structure: additional 2-OH for the dopamine−norepinephrine pair, catechol versus the 5-OH indole ring for the dopamine−serotonin pair. This difference may not be confined to the direct difference in the interactions with the receptor side chains. The chemical difference may have an implicit effect, as well: the bioactive conformation may (and probably does) differ from the local free energy minimum structures, and the readiness for a distortion to the bioactive conformation may also depend on the chemical structure.

The following question may, however, emerge: is our complicated combined DFT/ab initio/MC approach necessary at all for determining the in-solution relevant conformations and relative free energies. For a comparison, molecular mechanics geometry optimizations and energy calculations have also been performed using three values for the dielectric constant, ϵ (4r, 1r, and 1, respectively), shown in Table 5. The basic conclusion considering the values from Tables 1−3 is that the relative T and G2 free energies considerably decrease and increase, respectively, as compared to the gas-phase internal energies. In molecular mechanics optimizations, the three different forms for ϵ are decisive, because even with an NB cutoff = 8.0 Å almost all nonbonded intramolecular interactions were considered in the $SerH^+$ cation. The $\epsilon = 4r$ functional form mimics the solvent effects to a greater extent than the other two approximations. Since the CHELPG charges were derived by means of the in-solution wave function, this charge set should be most logically combined with the $\epsilon = 4r$ parameter. The derived relative energies (first set) show small variations for T and G2 with the Tripos force field; therefore, these MM calculations cannot reproduce the trend in the relative conformational free energy in aqueous solution. The MMFF94 relative energy for T is in fair agreement with the DFT/MC value. In this case, however, the MMFF94 charges were used, which did not depend on the conformation and sometimes differ from the CHELPG charges very remarkably. For example, the CHELPG charges for N_{am} varied between −0.21 and −0.35, whereas the MMFF94 value is −0.85. Not even the sign agrees for $N_{pyrrole}$ (the CHELPG values varied in the range −0.40 to −0.42 as compared to an MMFF94 charge of +0.03).

The charge sensitivity of the relative free energy in solution clearly appears from the difference in the DFT/MC and MMFF94 predicted G2 values. In contrast, the MMFF94 parametrization reproduces very well the B3LYP/6-31G* gas-phase relative energies.

The torsional angles can be predicted with a deviation of 10° at most with both MM methods. Changes in the ϵ function lead to a remarkable shift of the calculated key torsional angles. By comparing the first sets with the IEF-PCM/B3LYP/6-31G* values and the third set with the B3LYP/6-31G* gas-phase optimized dihedral angles, the trends are reproduced. Overall, while the conformer geometries can be fairly determined for protonated serotonin, the relative free energies have not been reproduced with either MM force fields and parametrizations.

For examining the serotonin···5-HT2A receptor interactions, six protonated serotonin conformers were considered in the present modeling. Since the optimized stable conformers take geometries without a symmetry plane, all these conformers exist in pairs of mirror images with equal energies. The receptor, however, has a set stereochemistry, thus binding energies of the elements of the mirror-image conformers must be in general different due to different geometric fits to the receptor binding site. Two modes of the ligand binding in conformations of G1 and G2′ are shown in Figure 11. Calculated geometric parameters as well as interaction and distortion energies are summarized in Table 6.

Throughout the successive energy minimization, molecular dynamics step and repeated energy minimization of the ligand···receptor complexes, the ligands generally saved their original G1, G2, and T as well as the corresponding mirror image characters even in the bound complex (Table 6). In the altogether 29 different cases, however, remarkable G1′ to T′, T′ to G2′, G2′ to G1′, and G2′ to T′ conformational changes were noticed, as well.

In a molecular mechanics study only comparisons among distinct conformations of the same system have physical meaning. Thus, the properly calculated differences may have physical relevance. In Table 6, all EI values calculated on the basis of eq 5 are negative, indicating a stabilizing interaction. Those values, however, depend on the parametrization; therefore, a more realistic prediction can be made from the ΔEI values. By using this procedure, the relative binding energies of the different conformers can be obtained, allowing assignment of the more likely binding form. The most negative EI interaction energies are in the range of −35 to −43 kcal/mol with different ligand conformations. In its strongest binding mode, each conformer forms at least one

Table 5. Relative Energies/Free Energies (kcal/mol) and Torsion Angles (deg) for Protonated Serotonin from Different Approaches

	relative energies or free energies		
	G1	T	G2
ΔE(B3LYP/6-31G*), gas phase	0.	5.1	−0.8
ΔG(IEF-PCM/B3LYP+MC/CHELPG charges), solution	0.	0.4± 0.4	3.9 ± 0.3
ΔE(Tripos force-field, CHELPG charges)[a]	0.	−0.4, −2.2, −8.0	−0.2, −2.1, −7.0
ΔE(MMFF94 force-field and charges)[a]	0.	0.9, 2.9, 5.3	−0.1, −0.3, −1.0

	torsion angles		
	G1	T	G2
B3LYP/6-31G*, gas phase			
$C_3C_\beta C_\alpha N$	−52.1	173.2	57.7
$C_2C_3C_\beta C_\alpha$	113.1	107.0	94.3
IEF-PCM/B3LYP/6-31G*, solution			
$C_3C_\beta C_\alpha N$	−61.0	178.5	59.4
$C_2C_3C_\beta C_\alpha$	105.7	102.3	84.5
Tripos force-field, CHELPG charges[a]			
$C_3C_\beta C_\alpha N$	−58.4, −53.0, −43.5	179.5, 179.2, 177.1	61.2, 58.5, 57.7
$C_2C_3C_\beta C_\alpha$	110.5, 113.8, 122.8	107.9, 108.9, 111.1	90.4, 91.7, 95.4
MMFF94 force-field and charges[a]			
$C_3C_\beta C_\alpha N$	−66.4, −58.9, −49.8	180.1, 180.2, 179.0	67.3, 61.0, 57.8
$C_2C_3C_\beta C_\alpha$	104.0, 107.6, 116.1	96.6, 96.4, 102.5	80.8, 80.6, 85.7

[a] The three consecutive values provided for MM calculations were obtained in energy minimizations with parameters for the dielectric function, ϵ, and the nonbonded cutoff, NB as (ϵ=4r, NB=8.0 Å), (ϵ=1r, NB=12.0 Å), and (ϵ=1, NB=12.0 Å), respectively.

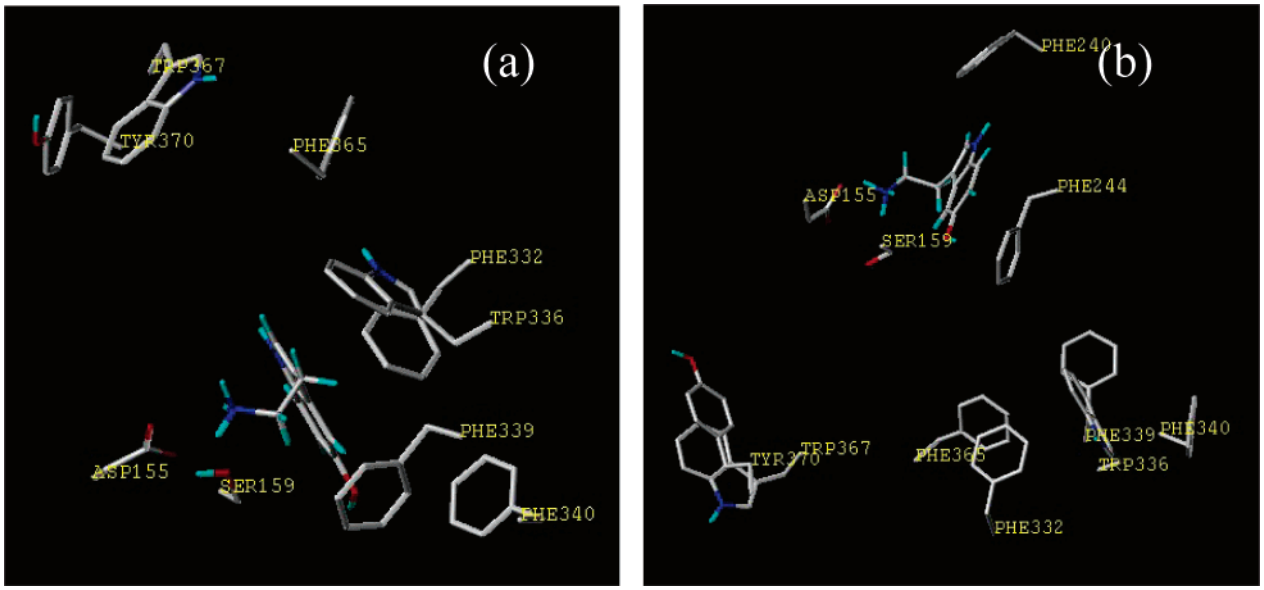

Figure 11. Receptor-bound forms of the ligand in the G1 (a) and G2′ (b) conformations.

strong $-N_{am}H^+\cdots{}^-OOC-$(Asp155) hydrogen bond with O···H distance of 1.6−2.0 Å. In the absence of such a bond, the EI values are remarkably less negative. These poses were found from starting arrangements involving $N_{am}\cdots{}^-OOC-$(Asp155) = 5−7 Å. Unless the $-N_{am}H^+\cdots{}^-OOC$ hydrogen bond was reestablished, the binding energy decreased (EI increased). The EI values form a range of 24 kcal/mol, indicating that each conformer has stronger and weaker binding modes.

Since in the strongest binding modes the different conformers of the $SerH^+$ ligand always form the $NH_3{}^+\cdots{}^-OOC$ hydrogen bond, the differences are attributed to the presence or absence of remarkable van der Waals interactions between the amino acid side chains and aromatics rings. Such an interaction was accepted as meaningful if at least one C···C distance between the indole ring of the ligand and the aromatic ring of the protein was less then 4 Å. In their most stable interactions with the receptor, the T′, G2′, and G2 conformers exhibited van der Waals interactions with amino acid residues Phe 240, 244 (TM V), Phe 339 (TM VI) and Trp 336, Phe 339, 340 (TM VI), respectively. In some binding modes of the G2′ and G1′ conformers (EI = −35.8 and −34.0 kcal/mol, respectively), the ligand interacts with the Phe365 and Tyr370 side chains, respectively, from TM VII. In weaker binding modes, van der Waals interactions

Table 6. Molecular Mechanics Energy (kcal/mol) and Geometry Terms Related to the Serotonin···5-HT2A Receptor-Model Interactions

	−EI	E(lig,dist)	ΔEI
G1	23.2−35.4	0.2−5.5	7.7−19.9
G1′	29.4−34.9	0.3−2.6	8.2−13.7
G2	29.9−41.0	0.5−1.5	2.1−13.2
G2′	32.8−41.4	1.0−2.0	1.7−10.3
T	29.3−37.4	0.3−3.3	5.7−13.8
T′	19.3−43.1	0.7−4.4	0.0−23.8

	torsion angles (deg)			
	ligand in adduct		optimized ligand	
	$C_2C_3C_\beta C_\alpha$	$C_3C_\beta C_\alpha N$	$C_2C_3C_\beta C_\alpha$	$C_3C_\beta C_\alpha N$
G1	95−173	−54 − (−72)	110.5	−58.4
G1′	−112 − (−129)	50−56	−110.5	58.4
G2	80−98	52−64	90.4	61.2
G2′	−88 − (−99)	−57 − (−82)	−90.4	−61.2
T	102−134	171−194	107.9	179.5
T′	−62 − (−143)	166−203	−107.9	−179.5

were noticed with Phe243 (TM V) and Trp367 (TM VII) residues, as well.

Two binding modes of the ligand in the G1 and G2′ conformations, establishing two medium-strong interactions (EI = −35.4 and −39.5 kcal/mol, respectively) with the receptor, are shown in Figure 11a,b. The cationic head of the ligand points toward the carboxylate group of Asp 3.32 (Asp155) in both cases. This interaction anchors the ligand and allows a motion of the rest of the molecule with a basically fixed location for the $-NH_3^+$ group, which is maintained in its place also by the interaction with Ser 3.36 (Ser159) found in experimental studies.[30] The indole ring interacts (Figure 11a) with several aromatic rings in the neighborhood, including Phe339, Phe340, Trp336, and Phe332 (TM VI), but it is far away from the aromatic part of Phe 7.38 (Phe365), Trp 7.40 (Trp367), and Tyr 7.43 (Tyr370). As mentioned above, interactions with these residues were found with some other ligand conformations. All these interactions were found important based on experimental studies by Roth et al.[29] In Figure 11b, as anticipated above, the side chain is still interacting with Asp and Ser, but the indole ring has moved to a different location because of its almost opposite φ_1 value: now the closest aromatic rings in the neighborhood are Phe244 and Phe240 in TM V.

As a summary of the docking studies, the rhodopsin-based 5-HT2A receptor model accounts for all the important ligand−receptor interactions found experimentally. The calculations provide an about 24 kcal/mol energy range for different binding modes, allowing G1, G2, and T conformations and their mirror images for the ligand. The binding mode and ligand conformation producing the most negative interaction energy do not necessarily correspond to the biologically active ligand conformation and the receptor activating binding mode. The diverse interaction energies and ligand conformations obtained in the docking study indicate, however, that neither steric hindrance nor activation problems should be expected when a protonated serotonin cation interacts with the 5-HT2A receptor in the binding cavity.

IV. Conclusions

Protonated serotonin takes two stable $C_{ring}C_\beta C_\alpha N$ gauche and one trans conformations in the gas phase. Transformation of the two gauche conformers by rotation about the $C_\beta-C_\alpha$ axis is hindered by barriers of about 2 kcal/mol, as calculated at the DFT level of theory (B3LYP) when the 6-31G* and 6-311++G** basis sets were applied. The gauche conformers are separated in energy by about 1 kcal/mol. The trans form is higher in energy by 6 kcal/mol than the most stable G2 conformer and is separated from the gauche structures by barriers of about 8 kcal/mol.

The in-solution conformational analysis was performed at the IEF-PCM level and by considering explicit solvent molecules within Monte Carlo simulations. Optimized geometries and internal energies were obtained at the IEF-PCM/B3LYP/6-31G* level. All calculations agree that two gauche and one trans side-chain conformations, at torsional angles close to those in the gas phase, represent the local minimum energy structures even in solution. A remarkable difference compared to the gas phase is, however, that the G1 to G2 barrier increased to 4 kcal/mol, whereas the T conformer is separated from the gauche forms by 4 kcal/mol. If an estimate for the relative thermal corrections is also considered, then the IEF-PCM/B3LYP/6-31G* calculations favor a gauche conformer, whereas the Monte Carlo simulations predict the trans form as the prevailing conformation. By considering, however the IEF-PCM/MP2/6-31G*//IEF-PCM/B3LYP/6-31G* results and the derived relative internal energies for the conformers, most calculations predict a nearly equal population for the G1 and T conformers in aqueous solution. Although any calculation predicts a conformational equilibrium in aqueous solution with detectable fractions for all three conformers, the authors prefer the MP2//B3LYP results because of the capacity of this theoretical level to predict conformer populations in fairly good agreement with the experimental results for a representative set of the 2-phenylethylamine family.

The solute is strongly hydrated by about three water molecules around the $-NH_3^+$ group with −9 to −17 kcal/mol interaction energy. Two water molecules, one for each, are expected to hydrate the pyrrole and the phenolic hydrogen atoms, as concluded from the analysis of the radial distribution functions.

Docking studies of the protonated ligand predicted both gauche and trans ligand conformers to favorably interact with the 5-HT2A receptor in its hypothesized binding cavity. The theoretical studies confirm the experimental results regarding strong interactions with the Asp155 and Ser159 residues (TM helix III) and the interactions of the indole ring with Phe, Trp, and Tyr side chains in TM V, VI, and VII helices. Neither steric hindrance nor activation problems should be expected when the protonated serotonin conformers interact with the 5-HT2A receptor with relative interaction energies up to about 24 kcal/mol.

Acknowledgment. The authors are indebted to Professor Jorgensen for permission to use the BOSS 4.2 program.

Supporting Information Available: B3LYP/6-31G* IR spectra in vacuo (Figure S1) and in solution at the IEF-PCM/B3LYP/6-31G* level (Figure S2) for G1, T, and G2 protonated serotonin, B3LYP optimized torsion angles for protonated serotonin in the gas phase (Table S1), selected wavenumbers in vacuo at the B3LYP/6-31G* level for protonated serotonin (Table S2), selected wavenumbers at the IEF-PCM/B3LYP/6-31G* level for protonated serotonin in aqueous solution (Table S3), and IEF-PCM/B3LYP/6-31G* CHELPG and RESP charges in aqueous solution (Figure S3) for the conformers considered (Tables S4 and S5, respectively). This material is available free of charge via the Internet at http://pubs.acs.org.

References

(1) (a) Vogelsander, B.; Godfrey, P. D.; Brown, R. D. *J. Am. Chem. Soc.* **1991**, *113*, 7864−7869. (b) Worth, G. A.; Richards, W. G. *J. Am. Chem. Soc.* **1994**, *116*, 239−250. (c) Nagy, P. I.; Durant, G. J.; Hoss, W. P.; Smith, D. A. *J. Am. Chem. Soc.* **1994**, *116*, 4898−4909. (d) Karpinska, G.; Dobrowolski, J. C.; Mazurek. A. P. *J. Mol. Struct. (THEOCHEM)* **1996**, *369*, 137−144. (e) Godfrey, P. D.; Brown, R. D. *J. Am. Chem. Soc.* **1998**, *120*, 10724−10732. (f) Kovalainen, J. T.; Christiaans, J. A. M.; Ropponen, R.; Poso, A.; Perakyla, M.; Vepsalainen, J.; Laatikainen, R.; Gynther, J. *J. Am. Chem. Soc.* **2000**, *122*, 6989−6996. (g) Kraszni, M.; Kokosi, J.; Noszal, B. *J. Chem. Soc. Perkin 2*, **2002**, 914−917. (h) Ramirez, F. J.; Tunon, I.; Collado, J. A.; Silla E. *J. Am. Chem. Soc.* **2003**, *125*, 2328−2340. (i) Raczynska, E. D.; Darowska, M.; Cyranski, M. K.; Makowski, M.; Rudka, T.; Gal, J. F.; Maria, P. C. *J. Phys. Org. Chem.* **2003**, *16*, 783−796.

(2) (a) Urban, J. J.; Cramer, C. J.; Famini, G. R. *J. Am. Chem. Soc.* **1992**, *114*, 8226−8231. (b) Alagona, G.; Ghio, C. *Chem. Phys*. **1996**, *204*, 239−249. (c) Urban, J. J.; Cronin, C. W.; Roberts, R. R. Famini, G. R. *J. Am. Chem. Soc.* **1997**, *119*, 12292−12299. (d) Nagy, P. I.; Alagona, G.; Ghio, C. *J. Am. Chem. Soc.* **1999**, *121*, 4804−4815. (e) Aliste, M. P.; Cassels, B. K. *J. Chem. Soc., Perkin 2* **2001**, 906−915. (f) Alagona, G.; Ghio, C. *Int. J. Quantum Chem*. **2002**, *90*, 641−656. (g) Nagy, P. I.; Völgyi, G.; Takács-Novák, K. *Mol. Phys*. **2005**, *103*, 1589−1601.

(3) (a) Nagy, P. I.; Alagona, G.; Ghio, C.; Takács-Novák, K. *J. Am. Chem. Soc.* **2003**, *125*, 2770−2785. (b) Snoek, L. C.; Van Mourik, T.; Simons, J. P. *Mol. Phys*. **2003**, *101*, 1239−1248. (c) Snoek, L. C.; Van Mourik, T.; Carcabal, P.; Simons, J. P. *Phys. Chem. Chem. Phys.* **2003**, *5*, 4519−4526.

(4) Van Mourik, T.; Emson, L. E. V. *Phys. Chem. Chem. Phys*. **2002**, *4*, 5863−5871.

(5) (a) Goodman & Gilman's: *The Pharmacological Basis of Therapeutics*, 9th ed.; Hardman, J. G., Limbird, L. E., Molinoff, P. B., Goodman Gilman, A., Eds.; McGraw-Hill: New York, 1996. (b) Foye's: *Principles of Medicinal Chemistry*, 5th ed.; Williams, D. A., Lemke, T. L., Eds.; Lippincott, Williams & Wilkins: Baltimore, MD, 2002.

(6) (a) Tota, M. R.; Candelore, M. R.; Dixon, R. A. F.; Strader, C. D. *Trends Pharmacol. Sci.* **1991**, *12*, 4−6. (b) Trumpp-Kallmeyer, S.; Hoflack, J.; Bruinvels, A.; Hibert, M. *J. Med. Chem.* **1992**, *35*, 3448−3462. (c) Strader, C. D.; Fong, T. M.; Tota, M. R.; Underwood, D. *Annu. Rev. Biochem. Soc.* **1994**, *63*, 101−132. (d) Lu, Z.-L.; Saldanha, J. W.; Hulme, E. C. *Trends Pharmacol. Sci*. **2002**, *23*, 140−146.

(7) Palczewski, K.; Kumasaka, T.; Hori, T.; Behnke, C. A.; Motoshima, H.; Fox, B. A.; Le Trong, I.; Teller, D. C.; Okada, T.; Stenkamp, R. E.; Yamamoto, M.; Miyano, M. *Science* **2000**, *289*, 739−745.

(8) Ballesteros, J. A.; Weinstein, H. *Methods Neurosci.* **1995**, *25*, 366−428.

(9) Liljefors, T.; Norrby, P.-O. *J. Am. Chem. Soc.* **1997**, *119*, 1052−1058.

(10) (a) Lee, C.; Yang, W.; Parr, R. G. *Phys. Rev. B* **1988**, *37*, 785−789. (b) Becke, A. D. *J. Chem. Phys.* **1993**, *98*, 5648−5652.

(11) Hehre, W. J.; Radom, L.; Schleyer, P. v. R.; Pople, J. A. *Ab Initio Molecular Orbital Theory*; Wiley: New York, 1986.

(12) (a) Møller, C.; Plesset, M. S. *Phys. Rev.* **1934**, *46*, 618−622. (b) Pople, J. A.; Binkley, J. S.; Seeger, R. *Int. J. Quantum Chem.* **1976**, *10s*, 1−19. (c) Krishnan, R.; Frisch, M. J.; Pople, J. A. *J. Chem. Phys.* **1980**, *72*, 4244−4245. (d) Pople, J. A.; Head-Gordon, M.; Raghavachari, K. *J. Chem. Phys.* **1987**, *87*, 5968−5975.

(13) Gaussian 03, Revision C.02. Frisch, M. J.; Trucks, G. W.; Schlegel, H. B.; Scuseria, G. E.; Robb, M. A.; Cheeseman, J. R.; Montgomery, J. A., Jr.; Vreven, T.; Kudin, K. N.; Burant, J. C.; Millam, J. M.; Iyengar, S. S.; Tomasi, J.; Barone, V.; Mennucci, B.; Cossi, M.; Scalmani, G.; Rega, N.; Petersson, G. A.; Nakatsuji, H.; Hada, M.; Ehara, M.; Toyota, K.; Fukuda, R.; Hasegawa, J.; Ishida, M.; Nakajima, T.; Honda, Y.; Kitao, O.; Nakai, H.; Klene, M.; Li, X.; Knox, J. E.; Hratchian, H. P.; Cross, J. B.; Bakken, V.; Adamo, C.; Jaramillo, J.; Gomperts, R.; Stratmann, R. E.; Yazyev, O.; Austin, A. J.; Cammi, R.; Pomelli, C.; Ochterski, J. W.; Ayala, P. Y.; Morokuma, K.; Voth, G. A.; Salvador, P.; Dannenberg, J. J.; Zakrzewski, V. G.; Dapprich, S.; Daniels, A. D.; Strain, M. C.; Farkas, O.; Malick, D. K.; Rabuck, A. D.; Raghavachari, K.; Foresman, J. B.; Ortiz, J. V.; Cui, Q.; Baboul, A. G.; Clifford, S.; Cioslowski, J.; Stefanov, B. B.; Liu, G.; Liashenko, A.; Piskorz, P.; Komaromi, I.; Martin, R. L.; Fox, D. J.; Keith, T.; Al-Laham, M. A.; Peng, C. Y.; Nanayakkara, A.; Challacombe, M.; Gill, P. M. W.; Johnson, B.; Chen, W.; Wong, M. W.; Gonzalez, C.; Pople, J. A. Gaussian, Inc., Wallingford, CT, 2004.

(14) McQuarrie, D. A. *Statistical Mechanics*; University Science Book: Sausalito, CA, 2000.

(15) Wong, M. W. *Chem. Phys. Lett.* **1996**, *256*, 391−399.

(16) (a) Cancès, E.; Mennucci, B.; Tomasi, J. *J. Chem. Phys*. **1997**, *107*, 3032−3041. (b) Cancès, E.; Mennucci, B. *J. Chem. Phys*. **1998**, *109*, 249−259. (c) Cancès, E.; Mennucci, B. *J. Chem. Phys.* **1998**, *109*, 260−266.

(17) Bondi, A. *J. Phys. Chem.* **1964**, *68*, 441−451.

(18) (a) Tomasi, J.; Persico, M. *Chem. Rev.* **1994**, *94*, 2027−2094. (b) Barone, V.; Cossi, M.; Tomasi, J. *J. Chem. Phys.* **1997**, *107*, 3210−3221.

(19) Amovilli, C.; Barone, V.; Cammi, R.; Cancès, E.; Cossi, M.; Mennucci, B.; Pomelli, C. S.; Tomasi, J. *Adv. Quantum Chem.* **1998**, *32*, 227−261.

(20) (a) Alagona, G.; Ghio, C.; Nagy, P. I. *Int. J. Quantum Chem.* **2004**, *99*, 161−178. (b) Nagy, P. I.; Takács-Novák, K. *Phys. Chem. Chem. Phys.* **2004**, *6*, 2838−2848. (c) Nagy, P. I. *J. Phys. Chem. B* **2004**, *108*, 11105−11117.

(21) Breneman, C. M.; Wiberg, K. B. *J. Comput. Chem.* **1990**, *11*, 361−373.

(22) (a) Bayly, C. I.; Cieplak, P.; Cornell, W. D.; Kollman, P. A. *J. Phys. Chem.* **1993**, *97*, 10269−10280. (b) Cornell, W. D.; Cieplak, P.; Bayly, C. I.; Kollman, P. A. *J. Am. Chem. Soc*. **1993**, *115*, 9620−9631.

(23) (a) Zwanzig, R. W. *J. Chem. Phys*. **1954**, *22*, 1420−1426. (b) Jorgensen, W. L.; Ravimohan, C. *J. Chem. Phys.* **1985**, *83*, 3050−3054.

(24) Jorgensen, W. L. *BOSS version 4.2*; Yale University: New Haven, CT, 2000.

(25) (a) Jorgensen, W. L.; Madura, J. D. *J. Am. Chem. Soc.* **1983**, *105*, 1407−1413. (b) Jorgensen, W. L.; Swenson, C. J. *J. Am. Chem. Soc.* **1985**, *107*, 1489−1496. (c) Jorgensen, W. L.; Gao, J. *J. Phys. Chem.* **1986**, *90*, 2174−2182. (d) Jorgensen, W. L.; Briggs, J. M.; Contreras, M. L. *J. Phys. Chem.* **1990**, *94*, 1683−1686.

(26) (a) Jorgensen, W. L.; Chandrasekhar, J.; Madura, J. D.; Impey, R. W.; Klein, M. L. *J. Chem. Phys.* **1983**, *79*, 926−935. (b) Jorgensen, W. L.; Madura, J. D. *Mol. Phys.* **1985**, *56*, 1381−1392.

(27) Jorgensen, W. L.; Maxwell, D. S.; Tirado-Rives, J. *J. Am. Chem. Soc.* **1996**, *118*, 11225−11236.

(28) Rajeswaran, W. G.; Cao, Y.; Huang, X. P.; Wroblewski, M. E.; Colclough, T.; Lee, S.; Liu, F.; Nagy, P. I.; Ellis, J.; Levine, B. A.; Nocka, K. H.; Messer, W. S., Jr. *J. Med. Chem.* **2001**, *44*, 4563−4576.

(29) Roth, B. L.; Shoham, M.; Choudhary, M. S.; Khan, N. *Mol. Pharmacol.* **1997**, *52*, 259−266.

(30) Almaula, N.; Ebersole, B. J.; Zhang, D.; Weinstein, H.; Sealfon, S. C. *J. Biol. Chem.* **1996**, *271*, 14672−14675.

(31) Sybyl 6.91, Tripos Inc., St. Louis, MO, 2003.

(32) (a) Halgren, T. A. *J. Comput. Chem.* **1996**, *17*, 490−519, 520−552, 553−586, 616−641. (b) Halgren, T. A.; Nachbar, R. B. *J. Comput. Chem.* **1996**, *17*, 587−615.

(33) Lynch, B. J.; Zhao, Y.; Truhlar, D. G. *J. Phys. Chem. A* **2003**, *107*, 1384−1388.

(34) (a) Orozco, M.; Jorgensen, W. L.; Luque, F. J. *J. Comput. Chem.* **1993**, *14*, 1498−1503. (b) Carlson, H. A.; Nguyen, T. B.; Orozco, M.; Jorgensen, W. L. *J. Comput. Chem.* **1993**, *14*, 1240−1249.

(35) One of the referees of this article raised the problems of MP2 "used with a small basis set", without hydrogen polarization, and of intramolecular BSSE that can be mistaken for dispersion. Concerning 6-31G* (a medium-size basis set), for protonated norepinephrine in the gas phase the MP2/6-31G* optimized structures and stabilities were fairly consistent with those obtained at the MP2/6-311++G** level.[3a] Furthermore those latter results were almost exactly superimposed to the minima of the MP2/6-311++G**//HF/6-31G*curve. An analogous trend was obtained by Nielsen et al.[36] for a related substituted ethylammonium in water, where extending the basis set from 6-31+G* to 6-311+G** did not lead to any significant difference. In that case, however, it was necessary to use diffuse functions to describe the anionic head of the zwitterion. Concerning BSSE, actually MP2 is known to be more prone than HF to intermolecular BSSE at least, error that remains almost constant despite basis set enlargement, as observed also in polyatomic cation−water interactions.[37]

(36) Nielsen, P. A.; Norrby, P.-O.; Liljefors, T.; Rega, N.; Barone V. *J. Am. Chem. Soc.* **2000**, *122*, 3151−3155.

(37) Alagona, G.; Biagi, A.; Ghio, C. *Mol. Eng.* **1992**, *2*, 137−152.

(38) Melandri, S.; Maris, A. *Phys. Chem. Chem. Phys.* **2004**, *6*, 2863−2866.

(39) Solmajer, P.; Kocjan, D.; Solmajer, T. *Z. Naturforsch.* **1983**, *38c*, 758−762.

(40) Nagy, P. I.; Dunn, W. J., III.; Alagona, G.; Ghio, C. *J. Phys. Chem.* **1993**, *97*, 4628−4642.

(41) Nagy, P. I.; Durant, G. J.; Smith, D. A. *J. Am. Chem. Soc.* **1993**, *115*, 2912−2922.

CT050088C